Electronic Supplementary Information

For

Morphology- and defect-coordinated prominent microwave absorption, thermal exhaustion, and electrical insulation in SnO_2@SnP_2O_7@$Sn_2P_2O_7$ hierarchical architectures

Xinyu Liu†, Siyu Xie†, Shiyang Cai†, Kang Fu†, Xiangyang Liu†, Lingling Lin†, Zhenjie Yu†, Guoxiu Tong * †, Wenhua Wu†

†College of Chemistry and Material Sciences, Key Laboratory of the Ministry of Education for Advanced Catalysis Materials, Zhejiang Normal University, Jinhua 321004, China.

*** Corresponding Authors:** E-mail: tonggx@zjnu.cn (G.X. Tong); Tel.: +86-579-82282269; Fax: +86-579-82282269.

Seen from Figure 8b1 and 8b2, matching constant (*Z*) varies in the following trend: $Z_{S4}<Z_{S2}<Z_{S1}\approx Z_{S5}<Z_{S4P}<Z_{S3}$ at 2~11 GHz; $Z_{S4}< Z_{S4P}< Z_{S5}\approx Z_{S2}<Z_{S1}<Z_{S3}$ at 11~18 GHz. The Z presents an upward trend with *f* with large values over 4~18 GHz. The prominent matching performance is mainly ascribed to inner stress/oxygen vacancy defects caused by [Sn^{2+}]. In addition to increasing permittivity and conductivity, P doping tunes the balance between conductivity loss and polarization loss.

While the AC takes on a weak resonance peak over 2.0~9.0 GHz and a strong resonance peak over 9.0~18.0 GHz, indicating that the EM wave absorption of the HAs mainly focuses on the 9.0~18.0 GHz. The AC values fluctuate in a small scale.

Attenuating constant (*AC*) increases in the following order: $AC_{S4P}<AC_{S5}\approx AC_{S3}\approx AC_{S4}<AC_{S1}\approx AC_{S2}$ at 2~13 GHz; $AC_{S2}\approx AC_{S1}<AC_{S5}<AC_{S4}<AC_{S3}<AC_{S4P}$ at 13~18 GHz. The high AC corresponds to the large absorption (or low RL_{min}, Table S1), meaning that more EM waves are dampened or converted into thermal energy as they enter absorbing layers. The strong attenuation capability is due to

the cooperative effects of multiple polarization loss, conductive loss, and multiple scattering as a result of defects and hierarchical architecture.

Matching constant (Z) and attenuating constant (AC) are two crucial factors, which determine the wide EAB and strong absorption. The values of Z and AC usually are obtained respectively from the expressions: $AC = \frac{\sqrt{2}\pi f}{c} \times \sqrt{(\mu''\varepsilon'' - \mu'\varepsilon') + \sqrt{(\mu''\varepsilon'' - \mu'\varepsilon')^2 + (\mu'\varepsilon'' + \mu''\varepsilon')^2}}$ and $Z = \left|\frac{Z_{in}}{Z_0}\right| = \left|\sqrt{\frac{\mu_r}{\varepsilon_r}} \tan h\left(j\frac{2\pi f d}{c}\sqrt{\mu_r \varepsilon_r}\right)\right|$. The Z presents an upward trend with f; while the AC takes on a weak resonance peak over 2~8 GHz and a strong resonance peak over 8~18 GHz.

Table S1. MWACs summarization of SnO_2-based absorption materials. [2,7–20,46,47]

Absorbers	Loading amount (%)	Optimal R_L value (dB)	f (GHz) (optimal R_L)	d_w (mm) (R_L < –10dB)	EAB (GHz) (R_L < –10 dB)	EAB/d (GHz/mm)	Ref.
SnO_2@ZnO	80	-23.5	9.20	12.0	3.50	0.29	7
Fe_3O_4@SnO_2 nanochains	50	-39.4	5.67	5.5	1.70	0.31	9
Fe-doped SnO_2@RGO	60	-29.0	16.50	5.3	2.70	0.51	11
SnO_2-graphene	50	-15.3	15.94	2.0	1.30	0.65	12
Ni/SnO_2	70	-21.7	8.60	3.0	2.80	0.93	13
Sb_2O_3/SnO_2/mica	20	-25.6	11.80	2.4	3.10	1.29	8
Fe_3O_4/SnO_2 nanorods	80	-27.4	16.72	2.0	2.60	1.30	10
core-shell Ni/SnO_2 composites	50	-45.0	13.90	1.8	3.80	2.11	14
embroidered ball-shaped SnO_2	70	-45.6	12.40	2.6	6.08	2.34	20
Ni-doped SnO_2@MWCNTs	33	-39.2	8.20	1.5	3.60	2.40	15
SnO_2@PPy hybrid aerogels	10	-46.1	10.24	3.0	7.28	2.42	17
SnO_2/Fe_3O_4/MWCNT	70	-42.0	10.90	1.5	3.80	2.53	16
honeycomb SnO_2 Foams	30	-37.6	17.10	2.0	5.60	2.80	46
Ni@void@SnO_2	50	-29.7	15.20	1.7	4.80	2.82	47
AgNWs-CoNi@$Sn(OH)_2$/SnO_2	50	-37.8	6.40	2.0	5.80	2.90	18
Fe doped SnO_2/C	33	-44.5	15.44	1.5	4.50	3.00	19
SnO/SnO_2 nanosheets	25	-37.6	15.20	1.4	4.30	3.07	2
Sn_2PO_4Cl S4P	50	-46.98	12.48	2.1	5.60	2.67	
SnO_2@SnP_2O_7@$Sn_2P_2O_7$-S1	50	-44.92	16.64	2.4	6.48	2.70	
SnO_2@SnP_2O_7@$Sn_2P_2O_7$-S2	50	-47.33	16.64	2.2	6.32	2.87	This
SnO_2@SnP_2O_7@$Sn_2P_2O_7$-S3	50	-39.09	17.68	2.7	6.72	2.49	work
SnO_2@SnP_2O_7@$Sn_2P_2O_7$-S4	50	-36.61	12.96	2.0	6.48	3.24	
SnO_2@SnP_2O_7@$Sn_2P_2O_7$-S5	50	-35.01	12.16	2.2	5.92	2.69	

Table S2. Heat conductance summarization of SnO_2-based composites.[21–24,26–29,48–60]

Filler	Matrix	Loading (%)	Heat conductance (W/m·K)	Ref.
SiO_2/SnO_2 nanofibers	SiO_2 aerogel	8	0.025	48
SnO	Polystyrene / unsaturated polyester	1	0.172	49
Sb-SnO_2/CM	poplypropylene	70	0.187	28
SnO_2/EG nanofluids	ethylene glycol	25	0.277	26
$CsCoPO_4$	Ceramics	100	0.35	21
MWCNTs/Sb-SnO_2	Thermoplastic polyurethane	10	0.36	29
SnO_2/rGO nanofluids	water	0.1	0.63	27
T-ZnO	silicone oil	70	0.83	50
b-Al_2O_3	epoxy resin	70	1.13	51
SnO_x/Si_3N_4 films	Ceramics	100	1.24	24
TiO_2/Fe/C	silicone	45	1.87	52
$SnO_2/Y_2O_3/ZrO_2$	Ceramics	100	1.98	23
Al_2O_3/Ni/C	silicone	30	2.84	53
$Ti_{0.8}Sn_{0.2}O_2$	ceramic	100	3.2	54
CNF/Fe_xO_y	silicone	30	3.22	55
Sn^{2+} doped fluorophosphate glass	ceramic	100	3.25	22
Fe-doped $CeO_2/Ce(OH)_3$	silicone	45	3.442	56
MgO/Ni/MWCNT	silicone	40	3.61	57
graphene foams	silicone	5	3.95	58
MgO/Co/C	silicone	50	4.09	59
GN/PPy/Al_2O_3	silicone	50	4.649	60
Sn_2PO_4Cl S4P	silicone	20	4.003	This work
$SnO_2@SnP_2O_7@Sn_2P_2O_7$-S1	silicone	20	3.835	
$SnO_2@SnP_2O_7@Sn_2P_2O_7$-S2	silicone	20	4.394	
$SnO_2@SnP_2O_7@Sn_2P_2O_7$-S3	silicone	20	4.413	
$SnO_2@SnP_2O_7@Sn_2P_2O_7$-S4	silicone	20	4.745	
$SnO_2@SnP_2O_7@Sn_2P_2O_7$-S5	silicone	20	4.265	

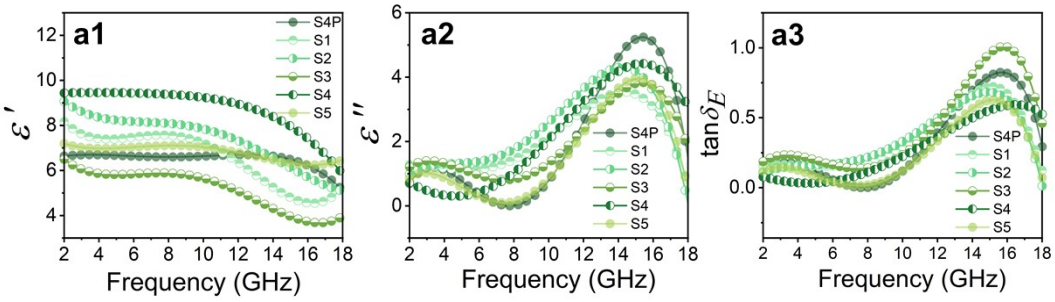

Figure S1. Frequency characteristics of the Sn_2PO_4Cl HAs (S4P) and $SnO_2@SnP_2O_7@Sn_2P_2O_7$ HAs (S1–S5): (a1) the real part (ε') and (a2) imaginary part (ε'') of relative complex permittivity, (a3) the dielectric loss ($\tan\delta_E$).

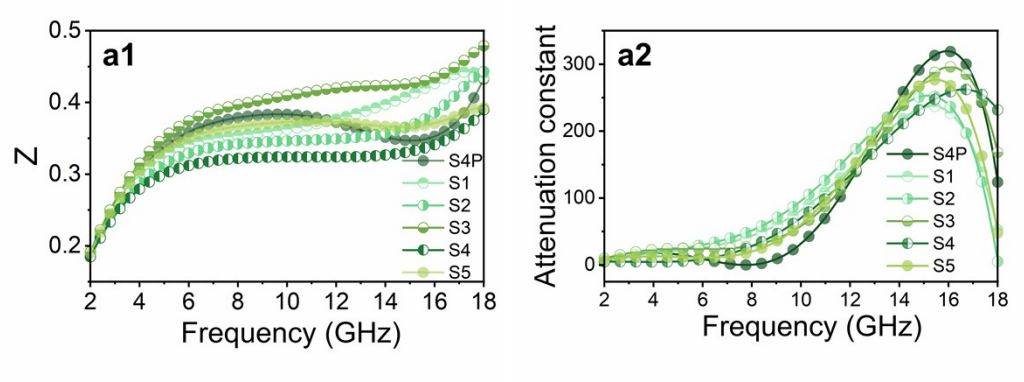

Figure S2. Frequency characteristics of the Sn_2PO_4Cl HAs (S4P) and SnO_2@SnP_2O_7@$Sn_2P_2O_7$ HAs (S1–S5): (a1) impedance matching (Z); (a2) attenuation constant (α).

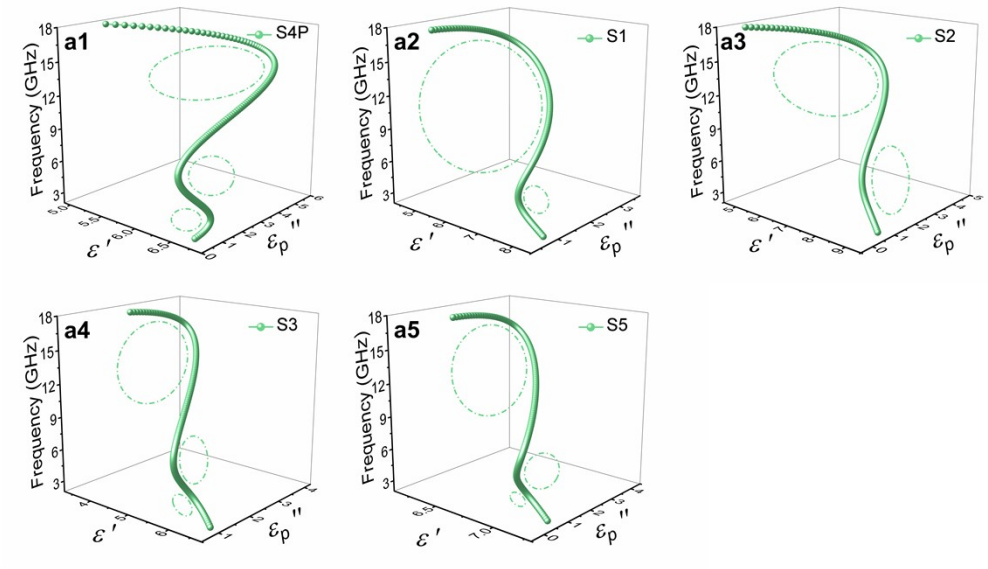

Figure S3. (a1–a5) Cole–Cole plots (ε' versus εp″) of the Sn_2PO_4Cl and SnO_2@SnP_2O_7@$Sn_2P_2O_7$ HAs.